



UNIVERSITY OF LEEDS

This is a repository copy of *Computational Design and Optimisation of Pin Fin Heat Sinks with Rectangular Perforations*.

White Rose Research Online URL for this paper:  
<http://eprints.whiterose.ac.uk/96442/>

Version: Accepted Version

---

**Article:**

Al-Damook, A, Kapur, N [orcid.org/0000-0001-8266-5038](https://orcid.org/0000-0001-8266-5038), Summers, JL et al. (1 more author) (2016) Computational Design and Optimisation of Pin Fin Heat Sinks with Rectangular Perforations. *Applied Thermal Engineering*, 105. pp. 691-703. ISSN 1359-4311

<https://doi.org/10.1016/j.applthermaleng.2016.03.070>

---

© 2016, Elsevier. Licensed under the Creative Commons Attribution-NonCommercial-NoDerivatives 4.0 International  
<http://creativecommons.org/licenses/by-nc-nd/4.0/>

**Reuse**

Unless indicated otherwise, fulltext items are protected by copyright with all rights reserved. The copyright exception in section 29 of the Copyright, Designs and Patents Act 1988 allows the making of a single copy solely for the purpose of non-commercial research or private study within the limits of fair dealing. The publisher or other rights-holder may allow further reproduction and re-use of this version - refer to the White Rose Research Online record for this item. Where records identify the publisher as the copyright holder, users can verify any specific terms of use on the publisher's website.

**Takedown**

If you consider content in White Rose Research Online to be in breach of UK law, please notify us by emailing [eprints@whiterose.ac.uk](mailto:eprints@whiterose.ac.uk) including the URL of the record and the reason for the withdrawal request.



[eprints@whiterose.ac.uk](mailto:eprints@whiterose.ac.uk)  
<https://eprints.whiterose.ac.uk/>

# Computational Design and Optimisation of Pin Fin Heat Sinks with Rectangular Perforations

Amer Al-Damook, J.L. Summers, N. Kapur, H.M. Thompson

School of Mechanical Engineering, University of Leeds, UK

Accepted for publication: 13<sup>th</sup> March 2016

## ABSTRACT

The benefits of using pin heat sinks (PHSs), where the pins are perforated with single, rectangular slotted or notched perforations, are explored computationally, using a conjugate heat transfer model for the conductive heat transfer through the heat sink and into the turbulent air flow over the heat sink. Results show that the heat transfer increases monotonically while the pressure drop decreases monotonically as the size of the rectangular perforation increases. Performance comparisons with PHSs with multiple circular perforations show that reduced manufacturing complexity of rectangular notched pins in particular, together with their favourable heat transfer and pressure drop characteristics, provide strong motivation for their use in practical applications. Detailed parameterisation and optimisation studies into the benefits of single rectangular notch perforations demonstrate the scope for improving heat transfer and reducing mechanical fan power consumption yet further by careful design of pin density and pin perforations in PHSs for specific applications.

NOMENCLATURE			
$A_c$	cross-sectional area of the flow passage of the heat sink, $m^2$	Re	Reynolds number
D	pin diameter of the pin fin heat sink, mm	T	temperature, °C
$D_h$	hydraulic diameter, m	$\Delta T$	temperature difference, °C
H	pin fin height, mm	U	air velocity, m/s
h	heat transfer coefficient, $W/m^2.K$	<b>Greek</b>	
k	turbulence kinetic energy, $m^2s^{-2}$	$\alpha$	fluid thermal diffusivity ( $m^2/s$ )
n	number of perforations	$\alpha, \beta, \beta^*$	turbulence model constant
N	number of pins	$\phi$	porosity $V_{void}=V$
L	heat sink length, mm	$\mu$	fluid viscosity (Pa·s)
Nu	Nusselt number	$\mu_t$	turbulent eddy viscosity, Pa.s
$P_{fan}$	fan power, W	$\rho$	fluid density ( $kg/m^3$ )
$\Delta p$	pressure drop, Pa	$\nu_t$	kinematic viscosity, $m^2/s$
Pr	Prandtl number	$\nu_t$	turbulent kinematic viscosity, $m^2/s$
$Pr_t$	turbulent Prandtl number	$\sigma_\epsilon$	k- $\epsilon$ turbulence model constant
Q	power applied on the base, W	$\sigma$	turbulence model constant for the k-equation
$S_z$	pin pitch in streamwise direction, mm	$\omega$	k- $\omega$ turbulence model constant

## INTRODUCTION

The increasing focus on energy efficiency and environmental sustainability, together with the need to achieve higher cooling rates, are providing strong drivers to optimise the performance of cooling technologies for a range of critical applications in e.g. the aerospace, avionics, automotive and nuclear industries, Sahin & Demir (2008,15). The electronics industry is also facing formidable challenges due to inexorable increases in power densities which make it increasingly difficult to ensure that micro-electronics temperatures remain below critical values above which failure modes associated with metal migration, void formation and inter-metallic growth degrade reliability, Gurrum et al (2004,17). These are driving rapid innovations in the thermal management of electronics towards promising technologies which include the use of highly conductive inserts to provide efficient pathways for heat removal, Hajmohammadi et al (2013), liquid cooling to increase cooling capacity, Hopton & Summers (2013,2), as

well as greater use of formal optimisation methods for component design, Najafi et al (2011, 19). Promising liquid cooling methods include on-chip cooling currently being used in the Aquasar system (1), which brings coolant right up to the main processor, and dielectric liquid immersion which removes heat by natural convection currents, Hopton & Summers (2013,2).

Cooling by convective heat transfer to air as it flows over a network of extended surface fins on a heat sink is still currently the most common cooling approach for microelectronics due to its low cost, availability and reliability, Zhou & Catton (2011,3). The fins offer a practical means of achieving a large total heat transfer surface area without excessive primary surface area and act as turbulence promoters thus further enhancing heat transfer rates. These heat sinks are usually designed to provide sufficient heat transfer rates to ensure that processor temperatures remain below the critical values, for minimal pressure loss, see e.g. the recent review by Nagarini et al (2014). The most widely used heat sink designs are those based on rectangular plate fin heat sinks (PFHSs) due to their simple structure and ease of manufacturing. These have been widely studied in the scientific literature and several studies have used experimental, Chiang (2005,5), and numerical, Najafi et al (2011,19), methods in order to improve heat transfer rates by limiting the regions where air flows smoothly through the heat sink channels. Recent attempts to overcome the latter include those of Kotcioglu et al (2013,20), who used periodically interrupted diverging and converging fins to enhance heat transfer through boundary layer disturbances and secondary mixing, and Kumar Das & Ghosh (2012) who considered the benefits of using multiple air streams to disturb the boundary layer. Najafi et al (2011,19) have used multi-objective Genetic Algorithms to optimise plate fin geometries for total heat transfer rate and annual costs.

Recent experimental and numerical studies have shown that perforating PFHSs can also offer substantial improvements in heat transfer with reduced pressure losses. The experiments of Dhanawade and Dhanawade (2010,14), for example, studied the effect of circular perforations parallel to the dominant air flow direction and found that perforations lead to reductions in the pressure loss by reducing both the size of the wakes behind the fin and the length of the recirculation zone around the lateral surfaces of the fins. These also showed that perforations generally increase the rate of heat transfer and that the optimum perforation diameter is a function of the applied heat flux density, with larger perforations being beneficial for low heat fluxes and smaller perforations better for high heat fluxes. Shaeri & Yaghoubi (2009,8,9) used numerical methods to study thermal air flows over arrays of solid and perforated plate fins, where the latter are perforated with one or more rectangular channels parallel to the dominant flow direction. They also found substantial improvements in heat transfer rate and reductions in total drag when perforations were used and noted that these benefits can be achieved with substantial reductions in fin weight, of up to 50%, for the cases considered.

Replacing plate fins by pins on Pinned Heat Sinks (PHSs) can be an effective enhancement to PFHSs since the pins hinder the development of the thermal boundary layer on smooth surfaces that limits the heat transfer rates in PFHSs, Zhou & Catton (2011). Previous investigations of heat transfer and pressure drops for air flows over PHSs have demonstrated clearly their superiority over PFHSs, Soodphakdee (2011). Attempts to further improve their performance have carried out design optimisation by exploring, for example, the effect of pin cross-sectional shape, Jonson & Moshfeghar (2001) and the benefits of combining plate and pin fins within compound heat sinks, Yang & Peng (2009,31).

In comparison with PFHSs, relatively few studies have considered the effect of perforations on heat transfer and pressure drops in PHSs and these have mainly focussed on the benefits of single perforations. Sahin & Demir (2008,15,16), for example, studied the effect of cross-sectional shape (circular or square) for in-line pin arrays while Amol et al (2013,17) considered the effect of staggered pin arrangements for singly-perforated pins of circular cross-section. More recently, Dai et al (2013) studied the benefits of micro-jets to improve heat transfer rate and reduce pressure drop by inducing flow separation in PHSs. Collectively, these studies have shown that, compared to solid pin systems, localised jet flows through perforations increase local heat transfer by increasing shear-induced mixing and, in addition, reduce overall pressure drop by reducing the size and strength of the recirculating zones that form behind the pins.

Al-Damouk et al (2015,18) have very recently used complementary experimental and numerical methods to explore the benefits of using multiple pin perforations within PHSs for the first time. They showed that the heat transfer rate increases monotonically with the number of pin perforations, while the pressure drop and fan power, required to overcome the pressure drop, both reduce monotonically; the location of the perforations were found to be much less influential. Pins with five perforations were found to increase heat transfer rate by over 10%, and reduce pressure drop by over 15%, compared with corresponding solid pin cases. These benefits are due not only to the increased surface area but also caused by the interactions of localised air jets through the perforations. Their conjugate heat transfer analysis showed, further, that improved heat transfer with pin perforations leads to significantly reduced processor case temperatures with the additional benefit of a reduction in the weight of the pins. Their experiments also revealed that practical considerations, including pin perforation alignment with the dominant flow direction and the quality of the pins' surface finish, can affect the heat transfer and pressure drop significantly.

The present study extends the recent work of Shaeri & Yaghoubi (2009,8,9) and Al-Damouk et al (2015,18) to consider the benefits of using pins with both internal rectangular perforations and with rectangular perforations etched into the top of the pins, see Figure 1. Since the latter may perhaps offer a more practical means of manufacturing PHSs with perforated pins, a multi-objective optimisation of the heat transfer and pressure drop in such systems is also presented. The paper is organised as follows. Section 2 describes the conjugate heat transfer model for the PHS problems under consideration and the numerical methods used to solve them. A comprehensive set of solutions is presented in Section 3 and conclusions are drawn in Section 4.

## **2. NUMERICAL METHODS**

### **2.1 Problem Description**

The PHS configurations considered here are shown in Figures 1 and 2 and based on those considered in the recent experimental study by Al-Damouk et al (2015), having base dimensions 50mm x 50mm x 2mm with an array of equally spaced 2mm diameter and 10mm height pins of circular cross-section. Thermal airflows past PHSs with pins based on three pins designs with rectangular perforations (henceforth referred to as 'slotted' pins) and three with rectangular notches removed from the top of the pin ('notched' pins) are compared with baseline cases with solid pins and pins with circular perforations considered by Al-Damouk et al (2015). The slotted pin designs have slot heights 3mm (3S), 6mm (6S) and 10mm (10S) while the notches have heights 2.5mm (2.5N), 5mm (5N) and 7.5mm (7.5N) with a

constant slot and notch width of 1mm. The porosities of the pin fins, defined as  $\phi = V_{\text{hole}}/V$  where  $V_{\text{hole}}$ , and  $V$  are the volume of the perforations and total pin volume respectively, range between 0 and 0.62.

## 2.2 Conjugate Heat Transfer Model

Thermal airflow through an aluminium PHS is analysed using Computational Fluid Dynamics (CFD). A schematic diagram of the flow domain used in the CFD analyses, with eight perforated pins in the air flow direction, is given in Figure 3 and consists of an inlet section, a test section over the PHS and an outlet section. The inlet air temperature is set to 25°C and the inlet air velocity is varied between 6.5m/s and 12m/s leading to Reynolds numbers in the range 3500-6580 based on a length scale given by the hydraulic diameter of the duct  $D_h = 2H.B/(H+B)$ , where  $H$  and  $B$  are height and width of duct in which the heat sink is located, respectively.

The rate of heat conduction through the aluminium heat sink is balanced by heat transfer by convection into the moving air stream, through a coupled boundary condition at the solid/fluid interface, as illustrated in Figure 4.

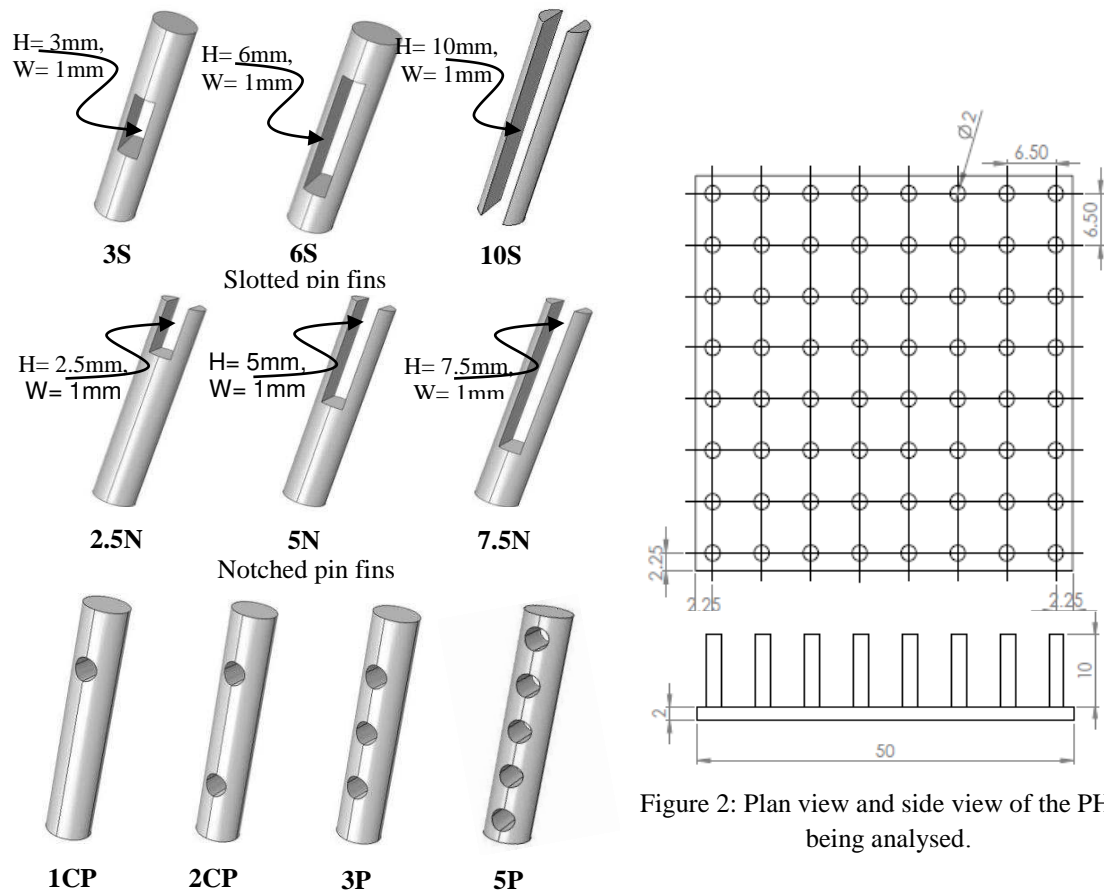
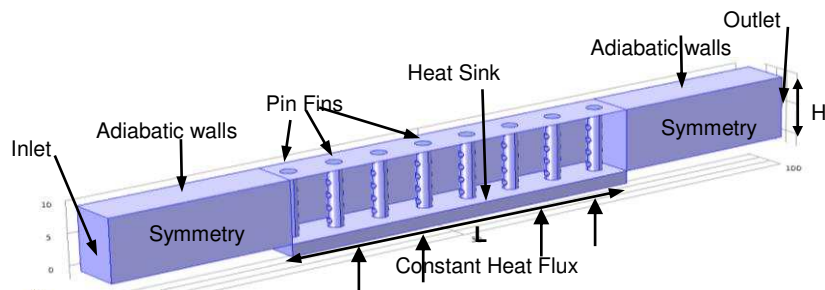


Figure 2: Plan view and side view of the PHSs being analysed.

Figure 1: Slot (S) and notch (N) perforations considered, together with circular (P) perforations considered by Al-Damouk et al (2015).



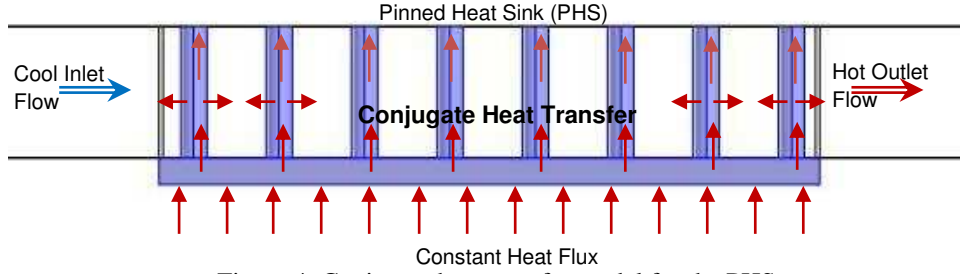


Figure 4: Conjugate heat transfer model for the PHS.

In the solid heat sink the temperature field  $T_s$  is obtained by solving the steady heat conduction equation

$$\nabla \cdot (k_s \nabla T_s) = 0$$

where  $k_s=202\text{W/mK}$  is the thermal conductivity of the aluminium heat sink. Turbulent flow through the PHSs is modelled using Reynolds-Averaged Navier-Stokes (RANS) equations, Zhou & Catton (2011), where the continuity, momentum and energy equations have variables decomposed into mean and fluctuating components, leading to:

$$\nabla \cdot \underline{\underline{U}} = 0$$

$$\frac{\partial \underline{\underline{U}}}{\partial t} + \nabla \cdot (\underline{\underline{U}} \underline{\underline{U}}) = \frac{1}{\rho} \nabla \cdot (\underline{\underline{\sigma}} - \rho \overline{\underline{\underline{U}}' \underline{\underline{U}}'})$$

where  $\underline{\underline{\sigma}} = -p \underline{\underline{I}} + \mu (\nabla \underline{\underline{U}} + [\nabla \underline{\underline{U}}]^T)$  and  $-\rho \overline{\underline{\underline{U}}' \underline{\underline{U}}'} = \mu_t (\nabla \underline{\underline{U}} + [\nabla \underline{\underline{U}}]^T) - 2/3(\rho k \underline{\underline{I}})$  are the

Newtonian and Reynolds Stress tensors respectively,  $\mu$  is the air viscosity,  $\rho$  its density,  $\underline{\underline{U}}$  and  $\overline{\underline{\underline{U}}}'$  the average and turbulent fluctuation velocity vectors respectively,  $p$  is the pressure and  $\underline{\underline{I}}$  the unit tensor.

The incompressible RANS equations are solved with the energy equation for the temperature field in the fluid,  $T_f$ , with a heat source  $\dot{Q}$  Watts, using the following equation

$$\frac{\partial T_f}{\partial t} + \underline{\underline{U}} \cdot \nabla T_f = \left( \frac{\nu}{Pr} + \frac{\nu_t}{Pr_t} \right) \nabla^2 T_f + \frac{\dot{Q}}{\rho C_p}$$

where  $C_p$  is the specific heat capacity of the air,  $Pr$  and  $\nu$  are the Prandtl number and kinematic viscosity of the air respectively and the subscript  $t$  indicates their turbulent counterparts.

Following Zhou & Catton [3], Leung & Probert [21] and Al-Damouk et al [18], the thermal airflow through the heat sink is modelled using the  $k-\omega$  SST model, which combines the accurate formulation of the  $k-\omega$  model in the near-wall region with the free-stream independence of the  $k-\epsilon$  one in the far field.

This has been shown to predict highly separated flows accurately in a number of previous validation studies, Menter [22], Zhou & Catton [3]. These studies also showed that the effects of radiative heat transfer can be neglected in flow over heat sinks and this simplifying assumption is also adopted here. Air density and viscosity are assumed to be constant and equal to those at the inlet temperature of 25°C.

The equations for the SST model are:

$$\frac{\partial(\rho k)}{\partial t} + \underline{U} \cdot \nabla(\rho k) = \tilde{P}_k - \beta^* \rho k \omega + \nabla \cdot [(\mu + \sigma_k \mu_t) \nabla k]$$

$$\frac{\partial(\rho \omega)}{\partial t} + \underline{U} \cdot \nabla(\rho \omega) = \alpha \rho S^2 - \beta \rho \omega^2 + \nabla \cdot [(\mu + \sigma_\omega \mu_t) \nabla \omega] + 2(1 - F_1) \rho \sigma_{\omega_2} \frac{1}{\omega} \nabla k \cdot \nabla \omega$$

where the blending function  $F_1$  is defined by

$$F_1 = \tanh \left( \left[ \min \left[ \max \left( \frac{\sqrt{k}}{\beta^* \omega y}, \frac{500 \nu}{y^2 \omega} \right), \frac{4 \rho \sigma_{\omega_2} k}{C D_{k\omega} y^2} \right] \right]^4 \right)$$

in which

$$C D_{k\omega} = \max \left( 2 \rho \sigma_{\omega_2} \frac{1}{\omega} \nabla k \cdot \nabla \omega, 10^{-10} \right)$$

The turbulent eddy viscosity is computed from

$$\nu_t = \frac{a_1 k}{\max(a_1 \omega, S F_2)}$$

where  $S$  is the invariant measure of the strain rate and  $F_2$  is a second blending function defined by

$$F_2 = \tanh \left( \left[ \max \left\{ 2 \frac{\sqrt{k}}{\beta^* \omega y}, \frac{500 \nu}{y^2 \omega} \right\} \right]^2 \right)$$

To limit the growth of turbulence in stagnation regions, a production limiter is used in the SST model.

Table 1: The boundary conditions of the conjugate heat transfer model.

$$P_k = \mu_t \frac{\partial u_i}{\partial x_j} \left( \frac{\partial u_i}{\partial x_j} + \frac{\partial u_j}{\partial x_i} \right) \rightarrow \tilde{P}_k = \min(P_k, 10 \beta^* \rho k \omega)$$

Locations	Fluid Conditions	Thermal Conditions	Locations	Fluid Conditions	Thermal Conditions
<b>Inlet</b>	$6.5 \leq U \leq 12 \text{ m/s}$	$T_f = 25^\circ\text{C}$ constant	<b>Bottom wall of heat sink</b>	$U=0$	$\dot{Q}=50\text{W}$ constant
<b>Right and left sides (symmetry)</b>	$\frac{du}{dy} = 0$	$\frac{dT}{dy} = 0$	<b>Pressure outlet</b>	$P=0$	$\frac{dT}{dx} = 0$
<b>Top wall and other walls</b>	$U=0$	$\frac{dT}{dz} = 0$	<b>Pin heat sink</b>	$U=0$	$k_{\text{air}} \cdot \frac{dT_{\text{air}}}{dn} = k_s \cdot \frac{dT_s}{dn}$

The constants for this model are:  $\beta^* = 0.09$ ,  $\alpha_1 = 5/9$ ,  $\beta_1 = 3/40$ ,  $\sigma_{k1} = 0.85$ ,  $\sigma_{\omega_1} = 0.5$ ,  $\alpha_2 = 0.44$ ,  $\beta_2 = 0.0828$ ,  $\sigma_{k2} = 1$ ,  $\sigma_{\omega_2} = 0.856$ .

A commercial Finite Volume Method-based code, ANSYS FLUENT [23] is used to solve the fully coupled momentum and energy equations, using second order upwinding, while continuity is satisfied using the SIMPLE method. The grid is composed of tetrahedral mesh elements to improve the quality of the numerical prediction near curved pin surfaces.

Table 1: The boundary conditions of the conjugate heat transfer model.

### 2.3 Boundary Conditions

The computational problem is reduced in size by exploiting the symmetry of the PHS to apply symmetry boundary conditions (Table 1) along the sides of the channel so that the conjugate heat transfer model is solved for a system of equally spaced pins aligned with the dominant flow direction, Figure 3. Along the bottom wall of the heat sink, a constant heat flux  $\dot{Q}=50W$  is applied and no-slip conditions  $U=0$  are imposed along the heat sink walls. A pressure outflow boundary condition is imposed at the outlet boundary. All remaining walls are considered to be adiabatic.

### 2.4 Post Processing

In addition to the thermal airflow throughout the PHSs, the CFD analysis is used to determine the Nusselt number,  $Nu$ , pressure drop,  $\Delta p$ , mechanical fan power,  $P_{fan}$ , and CPU temperature,  $T_{case}$  [32]. The average heat transfer coefficient,  $h$ , and Nusselt number,  $Nu$ , are defined by

$$h = \frac{\dot{Q}}{A_S [T_W - (\frac{T_{out} + T_{in}}{2})]}, \quad Nu = \frac{hL}{k_{air}}$$

where the area  $A_S$  is based on either the projected base area,  $A_P$ , or total wetted surface area,  $A_T$ , of the heat sink which includes the pin and perforation surface areas,  $T_W$  is the heat sink temperature at its upper surface,  $T_{in}$  and  $T_{out}$  are the average inlet and outlet air temperatures respectively.

The fan power required to drive the air through the heat sink, ignoring losses due to fan inefficiency, is defined by [31]

$$P_{fan} = U_{air} \cdot A \cdot \Delta p$$

where  $U_{air}$  is the inlet air velocity and  $A$  is the cross-sectional area of the flow passage of the heat sink  $= H \cdot S_z \cdot (N-1)$ , where  $S_z$  is the uniform pin spacing.

## 3. RESULTS AND DISCUSSION

### 3.1 Effect of Grid Density

Numerical solutions of the conjugate heat transfer model are obtained on a series of grids for both the solid and perforated pin fin cases shown in Figure 1 and the effect of grid resolution on  $Nu_T$ ,  $T_{case}$  and  $\Delta p$  are shown in the Appendix in Table A.1. For solid pin fins increasing the number of cells beyond 124,000 leads to a less than 3% variation in the quantities of interest, whereas for slotted and notched pin fins, increasing the number of cells beyond 116,000 and 117,000, respectively results in less than 2% variation in these parameters. All results reported subsequently have used these appropriate levels of grid refinement for solid and perforated pin fin cases.



### 3.2 Validation with Previous Studies

The numerical approach used here has recently has been shown to agree well with previous experimental and numerical studies of flows past PHSs with solid and circularly perforated pins, Al-Damouk et al (2015). Figure 5 compares the present study's predictions of the thermal resistance,

$R_{th} = \frac{(T_{case} - T_{in})}{\dot{Q}}$  of a solid PHS with the experimental results of Jonsson & Moshfegh [25] and the numerical data of Zhou & Catton [3] for  $6.5\text{m/s} \leq U_{in} \leq 10\text{m/s}$ . The agreement is generally very good, with a maximum discrepancy between these studies less than 3%.

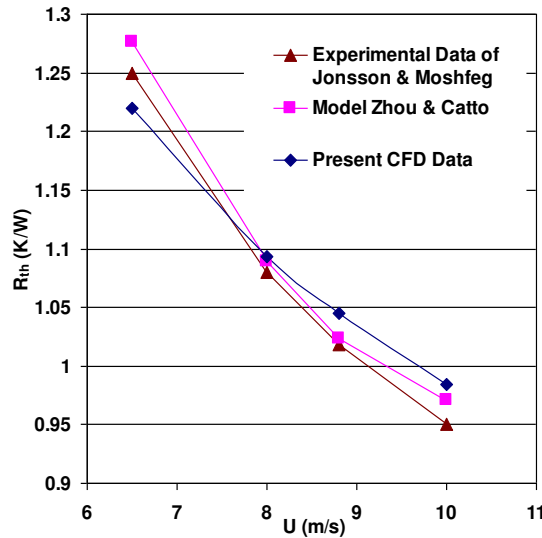


Figure 5: Comparison of thermal resistance predictions with CFD results of Zhou & Catton [3], and experimental data of Jonsson & Moshfegh [25].

### 3.3 Effect on Pressure Drop and Fan Power Consumption in PHSs

Figures 6 and 7 show numerical predictions of the effect of slot and notch perforations on  $\Delta p$  and  $P_{fan}$  respectively. Data is presented for the six slot and notch perforations shown in Figure 1 and compared against the benchmark PHS with solid pins. These show that both the slot and notch perforations reduce  $\Delta p$  and  $P_{fan}$  significantly and that the magnitude of these reductions increases monotonically with perforation size. For example, the 10S and 7.5N perforations lead to reductions in  $\Delta p$  and  $P_{fan}$  of approximately 40% and 35% respectively compared to solid pin PHSs.

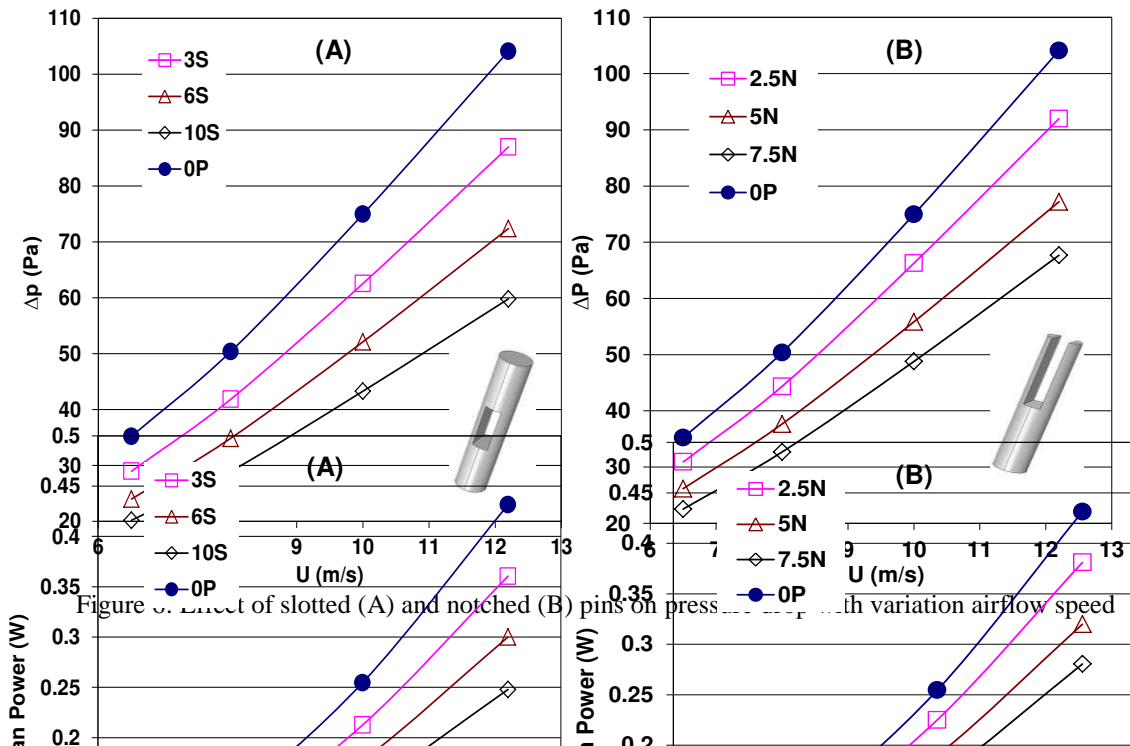
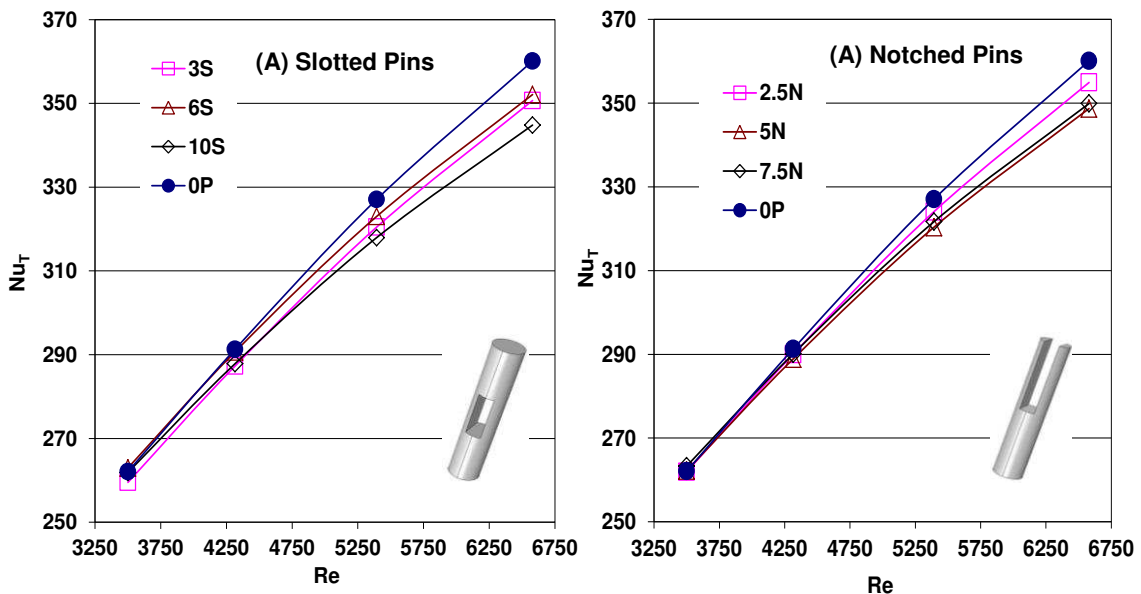


Figure 6: Effect of slotted (A) and notched (B) pins on pressure drop and fan power consumption with variation airflow speed

### 3.4 Effect on Heat Transfer Rate

Since one of the main design goals for PHSs is to achieve a high heat transfer rate at the minimum energy cost, Figure 8 shows the corresponding numerical predictions of Nusselt number, based on either the total PHS wetted surface area,  $Nu_T$ , or on the projected surface area,  $Nu_P$ . The latter may be a more effective measure of a heat sink's cooling capacity for a given PHS size. The data shows that both  $Nu_T$  and  $Nu_P$  increase approximately linearly with the Reynolds number and that  $Nu_T$  of the perforated pins is slightly smaller than for the solid pins. This contrasts with the values of  $Nu_P$ , which increase monotonically and strongly with perforation size. Since  $Nu_P$  is based on a constant projected area, these demonstrate that perforations improve the magnitude of the heat transfer and the magnitude of these increases is also significant: the values of  $Nu_P$  for the 10S and 7.5N perforations are typically 15% and 13% larger respectively than for solid pin PHSs. However, the fact that the values of  $Nu_T$  have decreased slightly means that the increase in heat transfer is slightly proportionately less than the increase in the total wetted surface area in the heat sink due to the perforations. These findings are consistent with the recent conclusions of Sara et al [26].



Collectively, Figures 6, 7 & 8 show that  $\Delta p$  and  $P_{fan}$  decrease monotonically and  $Nu_P$  increases monotonically with increasing perforation height,  $H$ .

The nature of the flow field in the vicinity of the slotted and notched perforations influences the pressure drop and heat transfer enhancements that they produce, Sara et al [26]. Figure 9 shows that the recirculating flow region behind the solid pins (0P) is reduced considerably by the addition of the perforations, which lead in turn to air jets flowing through them which enhance the local heat transfer rate and reduce the pressure drop across them.

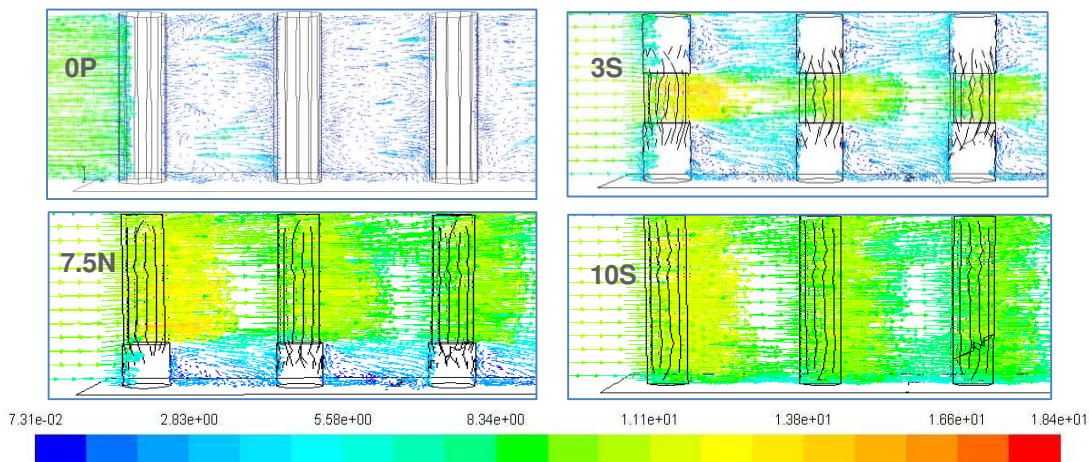


Figure 9: Comparison between predicted flow field in PHSs with solid pin fins and for pin designs 3S, 7.5N, and 10S. Viewing plane along pin centres.

### 3.5 Thermal Management of PHSs and Pin Weight Reductions

In many electronics applications systems, PHSs provide the cooling needed to keep processor temperatures below critical temperatures where thermally-driven failure mechanisms, including intermetallic growth, corrosion, metal migration and void formation, degrade reliability and reduce the mean-time-to-failure [27, 28]. Figure 10 presents numerical predictions of the average PHS base plate temperature,  $T_{case}$ , as a function of the fan power needed to overcome the pressure drop, for inlet air velocities in the range  $6.5\text{m/s} \leq U \leq 12\text{m/s}$ . Both sets of data show the consistent trend of requiring higher fan power in order to reduce  $T_{case}$  and that the improved heat transfer from the slotted and notched pins leads to lower CPU temperatures compared to solid pins, for a specific fan power. With the exception of

the 10S slot design, which differs in the sense that it effectively doubles the number of pins,  $T_{case}$  decreases monotonically with perforation area, PHSs with the slotted 6S and notched 7.5N pins, for example, typically have  $T_{case}$  values 4°C lower than for solid PHSs, for the same fan power input.

Since minimising the weight of consumer electronic devices is very important, previous studies have considered the optimization of pin fins in terms of maximising the heat transfer rate for a given fin weight or by minimising the weight for a specified heat transfer rate, Shaeri & Yagoubi [10]. The 3S, 6S and 10S slotted pins reduce the weight of the pin by 20%, 35% and 60% respectively while the corresponding reductions for the 2.5N, 5N and 7.5N notched pins are 15%, 30% and 45% respectively. Consequently, the heat transfer, pressure drop and fan power benefits of the 7.5N notched pins also provide a further benefit of a 45% reduction in pin weight.

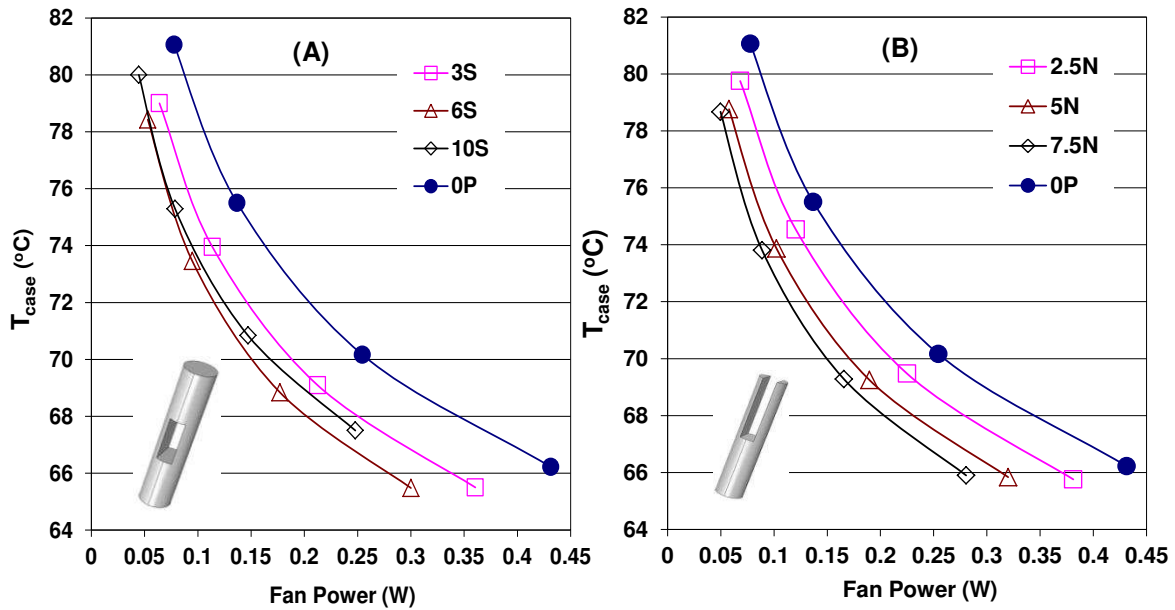


Figure 10: Effect of slotted and notched pin perforations on  $T_{case}$  as a function of input fan power. Figure 11 compares the surface temperatures of the solid pin fin heat sinks with those obtained with the 6S and 7.5N pin fins. In the former case, temperatures on the base plate vary between approximately 58.5°C and 71°C, whereas for the slotted (6S) and notched (7.5N) pins models the corresponding temperatures vary between approximately 54.5°C-70°C, 55.5°C-70°C, respectively. The temperatures on the pins are also significantly cooler, as indicated by the greater preponderance of blue regions on the new pin designs.

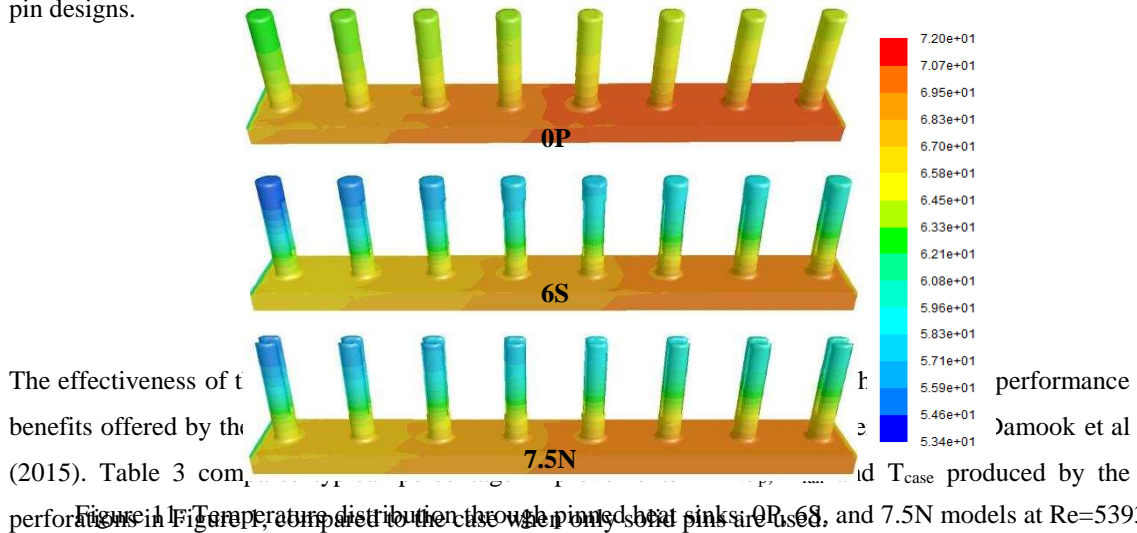


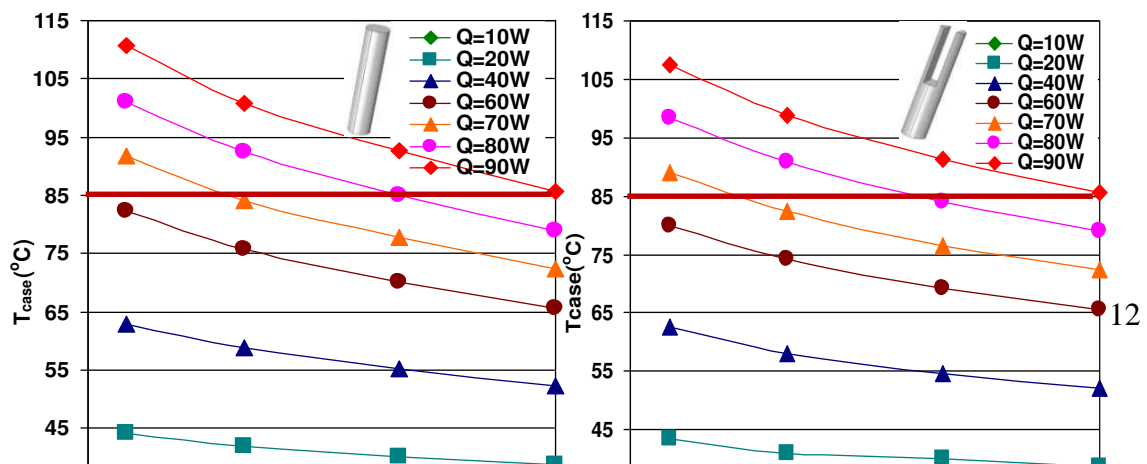
Table 3: Comparison in performance improvements for PHSs with pin designs shown in Figure 1.

Pin design	% increase in $A_T$	% increase in $Nu_p$	% reduction in $P_{fan}$	% reduction in $T_{case}$
1CP	5%	7	3	2
2CP	10%	17	7	5
3CP	15%	24	9	8
5CP	25%	35	16	10
3S	10%	8	17	2
6S	15%	15	31	2
10S	20%	17	42	0
2.5N	5%	4	12	1
5N	10%	8	26	2
7.5N	15%	13	35	2

These show that there is a compromise to be struck between the choice of perforations since the larger enhancements in heat transfer with multiple circular perforations come at the price of both a significantly increased power consumption and, perhaps most importantly, a much more complex manufacturing process. The above results suggest that PHSs with 7.5N notched pins may provide an effective, practical means of obtaining a good combination of heat transfer efficiency with a relatively low fan power consumption. All subsequent results focus on a parametric investigation of PHSs with notched pins.

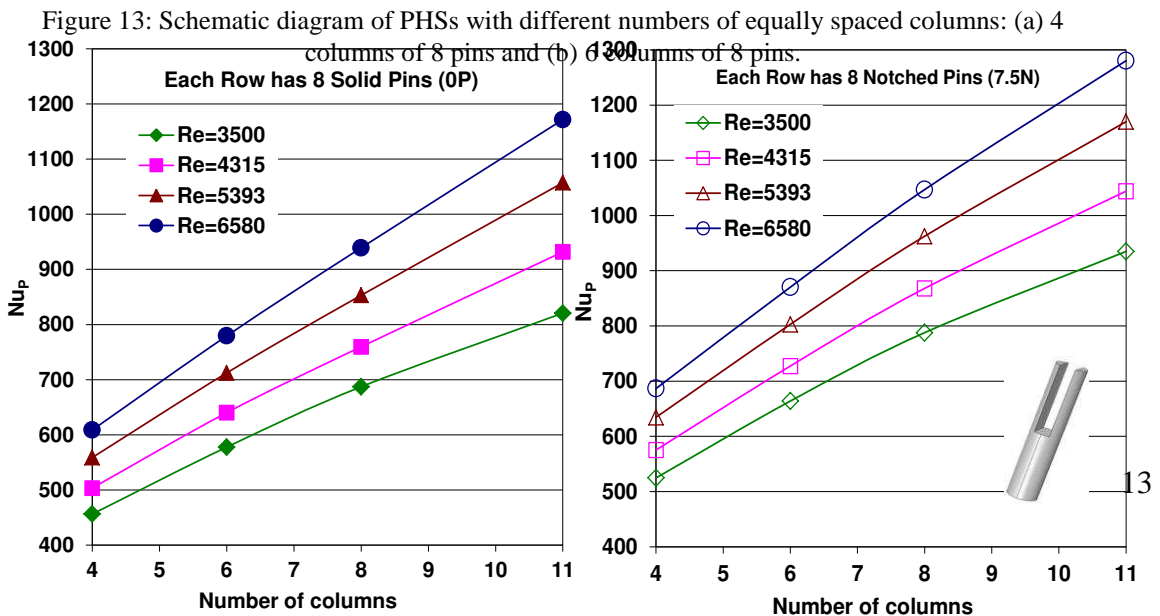
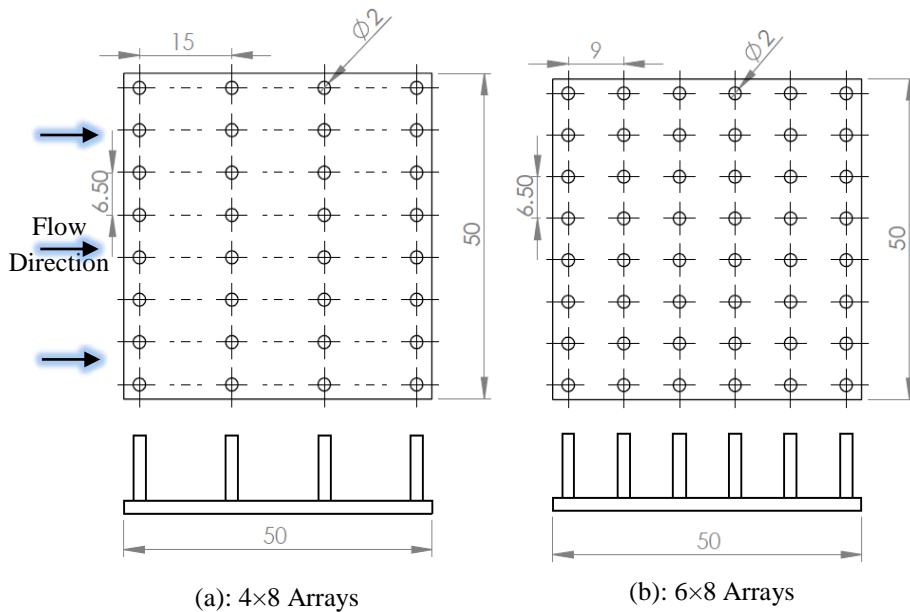
### 3.6 Effect of heating rate

Since modern CPUs have dynamically changing voltages, leading to variations in heating power  $\dot{Q}$ , at the base of a PHS, Figure 12 considers the effect of  $\dot{Q}$ , on  $T_{case}$  for a PHS with an 8x8 array of 7.5N notched pins. The heating power considered is in the range  $10W \leq \dot{Q} \leq 90W$ , typical of heating generated by PCs [28]. Taking  $85^\circ C$  as a critical  $T_{case}$  above which processor reliability degrades [27,28], Figure 12 shows that the critical temperature is exceeded for heating powers above 70W for air speeds below 8m/s, while the air speed must be above 10m/s for a power of 80W and above 12m/s if the power is greater than 90W.



### 3.7 Effect of pin density

The next series of results investigate the effect of varying the density of 7.5N notched pins on PHSs by investigating cases where each column of pins has 8 equally spaced pins, but varying numbers of equally spaced columns. Figures 13 (a) and (b) show two example PHSs with 4 and 6 columns of pins respectively. Figure 14 shows the effect of the number of columns of pins on  $Nu_p$  for PHSs with both solid and 7.5N notched pins, for a range of Reynolds numbers. It shows that  $Nu_p$  for the notched pins are typically at least 10% larger than for the solid pins and the values of  $Nu_p$  typically double as the number of columns is varied between 4 and 11.



The effect of pin density on the CPU temperature and fan power are shown in Figure 15. Results are plotted with respect to a reference critical temperature of 85°C. The results show that the increased heat conduction from the CPU, resulting from the higher pin densities, means that the CPU can be cooled below the critical temperature for a significantly lower fan power input,  $P_{fan}$ . For the solid pins, a fan power of 0.1W enables the CPU temperature  $T_{case}$  to be maintained below 85°C when 6 columns of pins are used whereas for 4 columns the CPU temperature of 100°C is well above the critical value. Using columns of 7.5N notched pins reduces the CPU temperature by between between 1°C and 3°C compared with solid pin fins, except for the case with 4 columns of pins where the temperatures for the two pin designs are very similar. The results also show that only 6 columns of the notched pins are needed for fan power inputs above 0.1W.

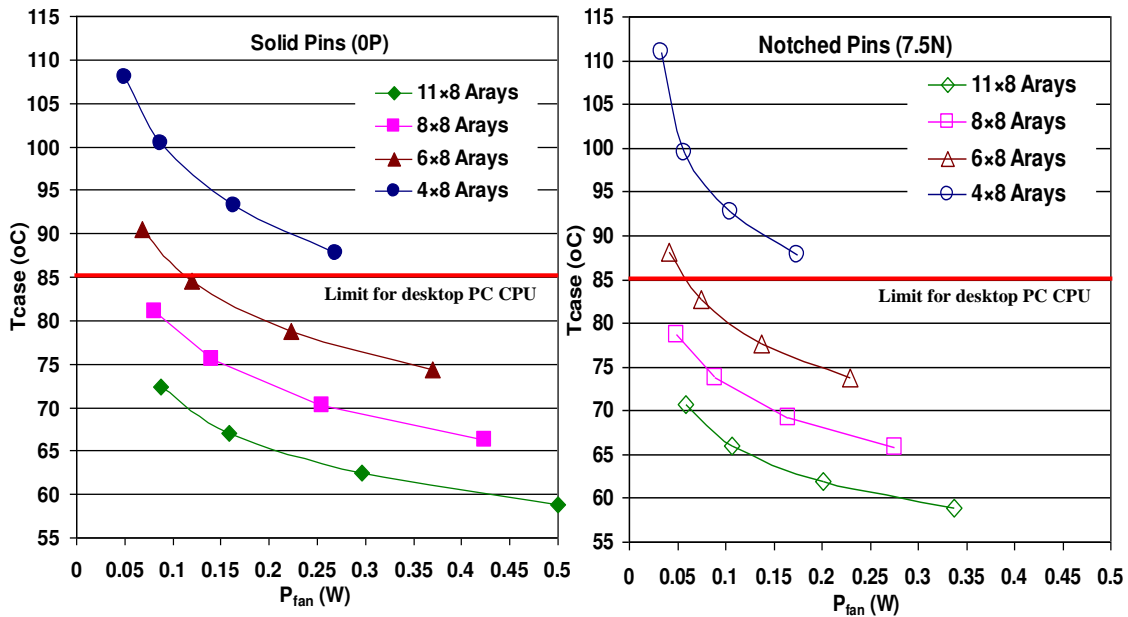
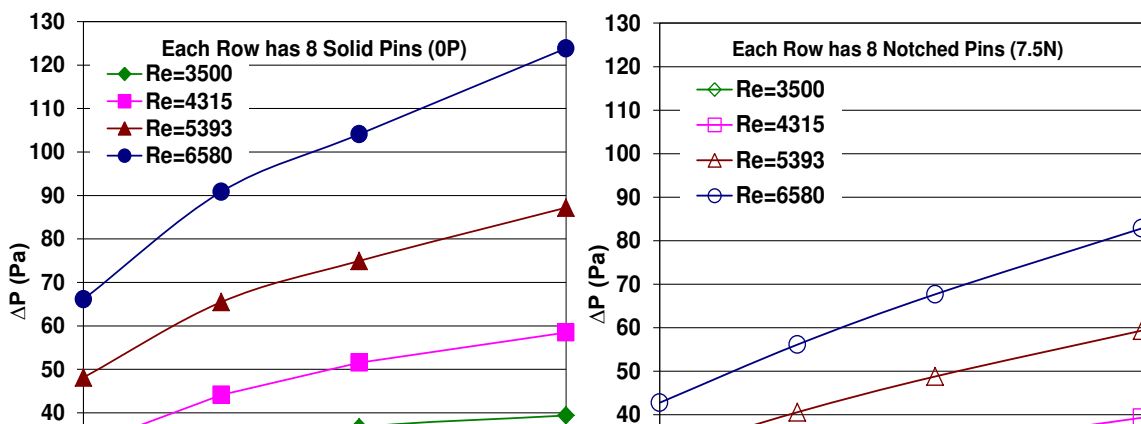


Figure 15: Effect pin density on  $T_{case}$  and fan power,  $P_{fan}$ , for PHSs with solid (0P) and notched (7.5N) pins.

Figure 16 shows the effect of the number of columns of pins on the pressure drop over the heat sink for both the solid and 7.5N notched pins. As expected, increasing the pin packing density increases  $\Delta p$  for both the solid and new pins models whereas the pressure drop for 7.5N pins is lower than for the solid pins. In both cases, halving the number of columns from 8 to 4 would reduce  $\Delta p$  by approximately 35%.



### 3.8 Optimum Design of Notched PHSs

PHSs are designed to maintain the processors below critical temperatures for minimal energy input into the system. This final section focusses on the optimisation of notched pins as a function of notch height,  $h$ , and width,  $w$ , for PHSs with an 8x8 array of pins with a constant pin spacing of 6.5mm in either direction. The multi-objective optimisation problem studied here is to minimise  $T_{\text{case}}$  and  $P_{\text{fan}}$  for  $2.5\text{mm} \leq h \leq 10\text{mm}$  and  $0.5\text{mm} \leq w \leq 1.5\text{mm}$  for a constant air inlet velocity,  $U_{\text{air}} = 8\text{m/s}$ . Since the above results has shown that minimising  $T_{\text{case}}$  and  $P_{\text{fan}}$  are in conflict with one another, the goal is to construct a Pareto front of non-dominated solutions, from which an appropriate compromise design can be chosen.

The Pareto front is obtained by building accurate metamodels of both  $T_{\text{case}}$  and  $P_{\text{fan}}$ , as a function of the design variables,  $h$  and  $w$ . Following a number of recent, successful optimisation studies, see e.g. Khatir et al (2015), the metamodels are built using the Moving Least Squares (MLS) method from a set of known values at specified Design of Experiments (DoE) points. The latter are obtained using an Optimal Latin Hypercube approach, which uses a permutation genetic algorithm to achieve a uniform spread of points within the design space. In the present study it is found that 30 DoE points are sufficient to provide accurate metamodels for both  $T_{\text{case}}$  and  $\Delta p$ . The MLS metamodels use a Gaussian weight decay function to determine the weighting of points in the regression analysis at each design point  $\underline{x}=(h,w)$ :

$$w_i(\underline{x}) = \exp(-\theta \|\underline{x} - \underline{x}_i\|^2),$$

where  $\|\underline{x} - \underline{x}_i\|^2 = (h - h_i)^2 + (w - w_i)^2$  is the Euclidean distance between the design point  $\underline{x}$ , at which the MLS metamodel is being evaluated, and the  $i$ th DoE point  $(h_i, w_i)$ , and  $\theta$  is the closeness of fit parameter. A large value of  $\theta$  ensures that the MLS metamodel reproduces the known values at the DoE points accurately, whereas a smaller value of  $\theta$  can reduce the effect of numerical noise on the MLS metamodel, Gilkeson et al (2014).

The values of  $\theta$  for the  $T_{\text{case}}$  and  $P_{\text{fan}}$  metamodels are determined by minimising the Root Mean Square Error (RMSE) between the predictions of the metamodels and the actual numerical predictions at the DoE points. Following Loweth et al (2011) and deBoer et al (2014), for each MLS metamodel, a  $k$ -fold cross-validation approach is used, where a large number of random samples of  $k$  points are removed from the 30 DoE points and the MLS metamodel rebuilt from the remaining  $(30-k)$  DoE points. The latter MLS metamodels are then used to calculate the RMSE at the removed DoE points, The average RMSE is then determined over a large number of folds; in the present study, 1000 folds with  $k=5$  are used. For the  $P_{\text{fan}}$



metamodel, this results in  $\theta_{opt}=41.7$  with a correlation coefficient between MLS and numerical predictions at the 30 DoE points,  $R=0.9996$ , and a maximum % difference of 1.2%. For the  $T_{case}$  metamodel,  $\theta_{opt}=16.7$  resulting  $R=0.9972$  and a maximum % difference of 1.6%. The optimised metamodels are shown in Figure 17, and demonstrate that the  $T_{case}$  and  $\Delta p$  minima occur on the domain boundaries.  $P_{fan}$  is reduced by increasing the notch area through increases to both  $h$  and  $w$ , whereas the  $T_{case}$  metamodel further highlights the importance of localised air jets through the perforation:  $T_{case}$  is reduced by increasing  $h$  and decreasing the slot width,  $w$ .

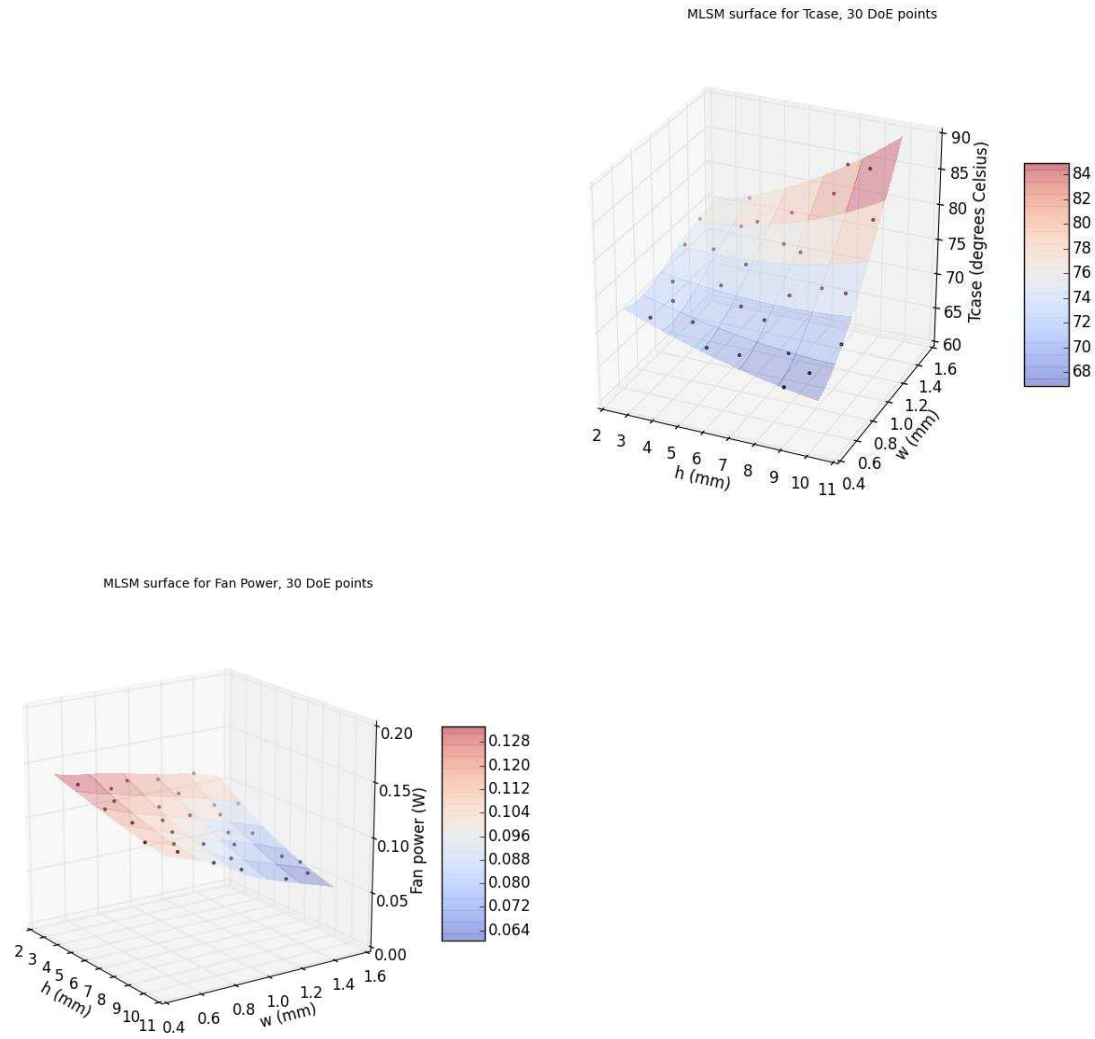


Figure 17: MLS metamodels for (a)  $P_{fan}$ ,  $\Delta p(\theta=41.7)$  and (b)  $T_{case}$  ( $\theta=16.7$ ).

The Pareto front is obtained by using the  $T_{case}$  metamodel to determine the design points ( $h,w$ ) at which  $T_{case}$  is a specified value and then using the  $P_{fan}$  metamodel to determine which of these design points has the smallest fan power consumption. The resultant Pareto front is shown in Figure 18, where the red crosses compare numerical predictions of  $T_{case}$  and  $P_{fan}$  against the Pareto front values obtained from the metamodels. These are generally in very good agreement with typical discrepancies of less than 1%.

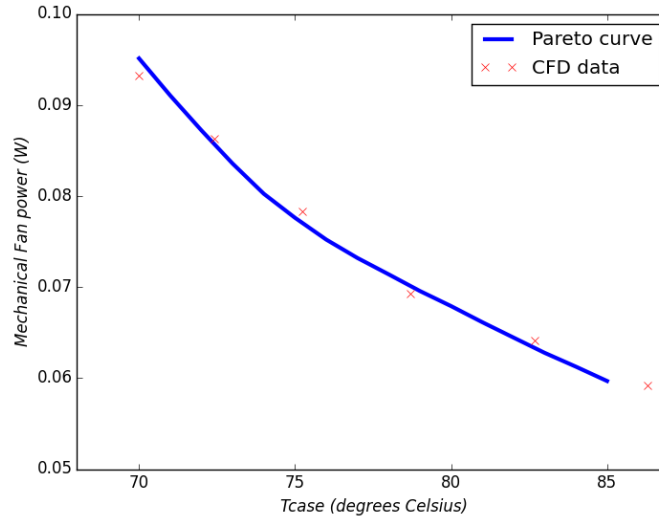


Figure 19: Pareto curve of  $T_{\text{case}}$  and mechanical fan power,  $P_{\text{fan}}$ , for an 8x8 PHS with slotted pins, with an inlet air speed of 8m/s.

The Pareto curve shows the compromise options that are available between a low  $T_{\text{case}}$  and a low  $P_{\text{fan}}$ . In the cases considered, the minimum  $P_{\text{fan}}$  that can be experienced while ensuring  $T_{\text{case}}$  is below the reference critical temperature of 85°C is approximately 0.06W, and this has to be increased by 30% (to 0.078W) and 60% (to 0.096W) to ensure  $T_{\text{case}}$  remain below 75°C and 70°C respectively.

## 5. CONCLUSIONS

Pinned heat sinks (PHSs) provide the cooling required in many critical applications, ranging from aero engines and nuclear reactors to computers and microelectronic devices. The present study considers the benefits of perforating the pins with rectangular slot or notch perforations and shows that both of these can provide significantly enhanced rates of heat transfer while simultaneously reducing the fan power required to create the air motion over the heat sink, compared to corresponding PHSs with solid pins.

These benefits have been shown to generally increase monotonically as the size of the perforation increases, and the largest slotted and notched perforations considered here have been shown to be able to increase heat transfer rate by over 10%, while at the same time reducing fan power consumption and pin weight by over 30% and 40% respectively. A comparison with PHSs with multiple circular perforations, Al-Damouk et al (2015), has shown that the former can achieve higher rates of heat transfer, due to the effect of multiple localised air jets, at the expense of higher fan power consumption and significantly increased manufacturing complexity. These results indicate that notched perforations may provide the most practical means of achieving the heat transfer and fan power benefits. The advantage of cutting slots from the top of the pins is that no pre-processing of the pins is required, Al-Damok et al (2015); from an existing heat sink either wire Electrical Discharge Machining could be used to directly cut into the slots, or a series of thin cutting discs mounted on a common shaft could be used with support to the pins provided through a jig. This would also retain the high thermal conductivity between the pin and the plate of a heat exchanger cast from a single block.

Pin density also has a significant influence on the heat transfer and pressure drop across PHSs. For PHSs with 7.5N slotted pins, results have shown that the increased conduction from higher densities of pins

enables the CPU to be cooled below the critical temperature for a significantly reduced fan input power,  $P_{fan}$ . A formal optimisation study of notched perforations has demonstrated the practical compromise that has to be struck between a low processor temperature  $T_{case}$ , which requires a narrow notch, and a low fan power needed to achieve the required rate of cooling, for which a wide notch is beneficial. The optimisation method provides a mechanism for designing the optimal perforations for specific heat transfer, fan power consumption and heat sink weight requirements.

## REFERENCES

1. IBM, Zurich, <http://www.zurich.ibm.com/st/energy/zeroemission.htm>.
2. Hopton, P. and Summers, J., Enclosed liquid natural convection as a means of transferring heat from microelectronics to cold plates. 29th IEEE Semiconductor Thermal Measurement and Management Symposium, 60-64, DOI: 10.1109/SEMI-THERM.2013.6526806.
3. Zhou, F. and I. Catton, Numerical Evaluation of Flow and Heat Transfer in Plate-Pin Fin Heat Sinks with Various Pin Cross-Sections. *Numerical Heat Transfer, Part A: Applications*, 2011. 60(2): p. 107-128.
4. Amol B. Dhumme and Hemant S. Farkade, Heat Transfer Analysis of Cylindrical Perforated Fins in Staggered Arrangement. *International Journal of Innovative Technology and Exploring Engineering (IJITEE)*, 2013. 2(5): p. 225-230.
5. K.T Chiang. Optimization of the design parameters of parallel-plain fin heat sink module cooling phenomenon based on the Taguchi method. *Int. Comm. Heat and Mass Transfer*, vol. 32(9), 1193-1201, 2005.
6. E.M. Sparrow & V.B. Grannis, Pressure drop characteristics of heat exchangers consisting of arrays of diamond-shaped pin fins. *Nnt. J. Heat and Mass Transfer*, 34(3), 589-600, 1991.
7. Q. Li, Z. Chen, U. Flechtner et al. Heat transfer and pressure drop characteristics in rectangular channels with elliptic pin fins. *Int. J. Heat and Fluid Flow*, 19(3), 245-250, 1998.
8. Shaeri, M.R. and M. Yaghoubi, Thermal enhancement from heat sinks by using perforated fins. *Energy Conversion and Management*, 2009. 50(5): p. 1264-1270.
9. Shaeri, M.R. and M. Yaghoubi, Numerical analysis of turbulent convection heat transfer from an array of perforated fins. *International Journal of Heat and Fluid Flow*, 2009. 30(2): p. 218-228.
10. Shaeri, M.R. and T.C. Jen, The effects of perforation sizes on laminar heat transfer characteristics of an array of perforated fins. *Energy Conversion and Management*, 2012. 64: p. 328-334.
11. Shaeri, M.R. and T.C. Jen, Turbulent Heat Transfer Analysis of a Three-Dimensional Array of Perforated Fins Due to Changes in Perforation Sizes. *Numerical Heat Transfer, Part A: Applications*, 2012. 61(11): p. 16.
12. Ismail, F., Effects of Perforations on the Thermal and Fluid Dynamic Performance of a Heat Exchanger. *IEEE Transaction on Component, Packaging and Manufacturing Technology*, 2013. p.1-8.
13. Md. Farhad Ismail, M.O. Reza, M.A. Zobaer, and Mohammad Ali, Numerical investigation of turbulent heat convection from solid and longitudinally perforated rectangular fins. *IEEE 5th BSME International Conference on Thermal Engineering*, 2013. p.497-502.
14. K. H. Dhanawade and H. S. Dhanawade, Enhancement of Forced Convection Heat Transfer from Fin Arrays with Circular Perforation. *IEEE, Frontiers in Automobile and Mechanical Engineering (FAME)*, 2010. p. 192-196.
15. Sahin, B. and A. Demir, Thermal performance analysis and optimum design parameters of heat exchanger having perforated pin fins. *Energy Conversion and Management*, 2008. 49(6): p. 1684-1695.
16. Sahin, B. and A. Demir, Performance analysis of a heat exchanger having perforated square fins. *Applied Thermal Engineering*, 2008. 28(5-6): p. 621-632.
17. Amol B. Dhumme and Hemant S. Farkade, Heat Transfer Analysis of Cylindrical Perforated Fins in Staggered Arrangement. *International Journal of Innovative Technology and Exploring Engineering (IJITEE)*, 2013. 2(5): p. 225-230.
18. Amer Al-damook, Kapur N., Summers J.L., Thompson H.M., An experimental and computational investigation of thermal airflows through perforated pin heat sinks, *Applied Thermal Engineering Journal*, 2015, 89, 365-376.
19. H. Najafi, B. Najafi, P. Hoseinpoori, Energy and cost optimization of a plate and fin heat exchanger using genetic algorithm. *Applied Thermal Engineering*, 2011, 31, pp 1839-1847.
20. I. Kotcioglu, A. Cansiz, M. Nasiri Khalaji, Experimental investigation for optimization of design parameters in a rectangular duct with plate-fins heat exchanger by Taguchi method. *Applied Thermal Engineering*, 2013, 50, pp 604-613.

21. Leung, C. W., & Probert, S. D., Heat-exchanger performance: effect of orientation. Applied energy, 1989. 33(4), 235-252.
22. Menter, F. R., Zonal Two Equation k- $\omega$  Turbulence Models for Aerodynamic Flows, AIAA 1993, p.93-2906.
23. ANSYS FLUENT User's Guide, 2011.
24. A. Bejan, Entropy Generation Minimization. New York: CRC, 1996.
25. Moshfegh, H. Jonsson B., Modeling of the Thermal and Hydraulic Performance of Plate Fin, Strip Fin and Pin Fin Heat Sinks-Influence of Flow Bypass. IEEE Transactions on Components and Packaging Technologies, 2001. 24(2): p.142-149.
26. O. N. Sara, T. Pekdemir, S. Yapici and H. Ersahan, Thermal Performance Analysis for Solid and Perforated Blocks Attached on a Flat Surface in Duct Flow. Energy Conversion & Management, 2012. 41(10): p. 1010-1028.
27. S. P. Gurrum, S. K. Suman and J. Y. K., Thermal Issues in Next-Generation Integrated Circuits, IEEE Transactions on device and materials reliability, 2004, vol. 4, no. 4, pp. 709-714.
28. Yuan, W., Zhao, J., Tso, C. P., Wu, T., Liu, W., Ming, T., Numerical simulation of the thermal hydraulic performance of a plate pin fin heat sink. Applied Thermal Engineering, 2012. 48, 81-88.
29. Çengel, Yunus A., and John M. Cimbala. Fluid Mechanics: Fundamentals and Applications. Boston: McGraw-Hill Higher Education, 2006.
30. Narayanan, A., Toropov, V. V., Wood, A. S., & Campean, I. F., Simultaneous model building and validation with uniform designs of experiments. Engineering Optimization, 2007. 39(5): p. 497-512.
31. Yang, Y. T., Peng, H. S., Investigation of planted pin fins for heat transfer enhancement in plate fin heat sink. Microelectronics Reliability, 2009. 49(2): p.163-169.
32. Holman, J. P.. Experimental Methods for Engineers, McGraw Hill Book Company, 10971, 8th edition, 2011.

## APPENDIX

Table A.1: The effect of grid resolution for solid, slotted, and notched PHSs.

<b>Solid Pins (0P) Cells</b>	<b>Nu<sub>T</sub></b>	<b>T<sub>case</sub> (°C)</b>	<b>ΔP (pa)</b>
98104	348.2	67.4	107.1
124092	360.1	66.2	104.0
134035	362.3	66.3	103.8
171059	367.0	65.6	103.6

<b>Slotted Pins (3S)</b>	<b>Nu<sub>T</sub></b>	<b>T<sub>case</sub> (°C)</b>	<b>ΔP (pa)</b>	<b>Slotted Pins (6S)</b>	<b>Nu<sub>T</sub></b>	<b>T<sub>case</sub> (°C)</b>	<b>ΔP (pa)</b>
96390	336.1	67.3	85.7	93081	331.8	68	72.6
116295	350.6	65.5	86.9	115049	352.1	65.5	72.3
136631	363.2	64.6	86.1	131792	356.3	65.4	72.5
179951	372.0	63.3	85.3	168786	360.2	63.8	70.8
<b>Slotted Pins (10S)</b>	<b>Nu<sub>T</sub></b>	<b>T<sub>case</sub> (°C)</b>	<b>ΔP (pa)</b>	<b>Notched Pins (2.5N)</b>	<b>Nu<sub>T</sub></b>	<b>T<sub>case</sub> (°C)</b>	<b>ΔP (pa)</b>
97520	330.6	69.4	60.6	98594	347.7	66.4	93.6
109380	344.8	67.5	59.8	117261	354.9	65.8	91.9
134056	351.8	66.9	58.8	139076	361.9	65.5	91.0
164775	357.0	65.9	58.6	170039	366.3	64.6	91.2
<b>Notched Pins (5N)</b>	<b>Nu<sub>T</sub></b>	<b>T<sub>case</sub> (°C)</b>	<b>ΔP (pa)</b>	<b>Notched Pins (7.5N)</b>	<b>Nu<sub>T</sub></b>	<b>T<sub>case</sub> (°C)</b>	<b>ΔP (pa)</b>

95008	336.7	67.4	78.8	98594	347.5	66.3	66.9
115100	348.7	65.8	77.4	117261	349.9	65.3	66.7
134112	358.7	65.1	77.7	139076	361.0	64.5	66.3
171112	365.7	64.2	77.3	170039	364.4	64.1	66.1